Available online at www.sciencedirect.com
ScienceDirect
Journal of Sound and Vibration 314 (2008) 672–692
JOURNAL OF SOUND AND VIBRATION
www.elsevier.com/locate/jsvi

Comparison of statistical and interval analysis for the energy flow uncertainties in structural vibrating systems

Stefano Gabriele[a], Antonio Culla[b,*]

[a]Department of Structures, University "Roma Tre", Via V. Volterra 62, 00146 Rome, Italy
[b]Department of Mechanics and Aeronautics, University of Rome, "La Sapienza", Via Eudossiana 18, 00184 Rome, Italy

Received 21 July 2006; received in revised form 1 January 2008; accepted 9 January 2008
Handling Editor: C Morfey
Available online 4 March 2008

Abstract

In this paper the energy flow confidence between two structural multimodal systems coupled by a joint with uncertain parameters is computed by two different methods. The first one assumes that the joint parameters perturbed randomly: the statistical moments of the energy flow are calculated by an analytical procedure. The second one uses interval analysis. The joint parameters are considered interval variables and the interval of the energy flow is determined. The properties of the statistical and interval solution are investigated and compared.

1. Introduction

In studying predictive methods of structural vibrations, a difficulty arises in modelling the uncertainties of the physical parameters. The variability is generally more pronounced for the stiffness and damping parameters of a complex structure than for its geometry. In fact, these uncertainties are due to some manufacturing process of the structure. While the dimensions of each part of a complex structure are subjected to a strict check, on the contrary the production of the material and the assembly (welding, bolting, jointing by rivets, etc.), is in general subjected to less control.

Generally, besides uncertainties in the parameters of each structure, there is a lack of information associated with the junctions or those points of the structure where physical singularities exist (invisible damages, cracks, etc.).

The study of the coupling of multimodal systems is an interesting topic for both low-medium frequency and high-frequency problems. Moreover, investigation of the energy flows between mechanical systems becomes fundamental when the study of high-frequency problems (the response of structures or acoustic cavities excited by broad band forces) imposes the use of a statistical energy procedure to solve them (e.g. statistical energy analysis—SEA) [1–11].

*Corresponding author. Tel.: +39 6445 85556; fax: +39 6484 854.
E-mail address: antonio.culla@uniroma1.it (A. Culla).

0022-460X/$ - see front matter © 2008 Elsevier Ltd. All rights reserved.
doi:10.1016/j.jsv.2008.01.036

The basic idea is to find the response of a complex structure, a set of subsystems coupled together, by the knowledge of the response of each. Two mathematical models are used to describe the same physical phenomenon. The first is the classical model: a set of differential equations and boundary conditions describe the behaviour of the whole system. The second one is a set of equations, not necessarily differential, describing the interaction between the subsystems rather than the dynamic balance between infinitesimal volumes. It is considered here that the joints between subsystems are subsystems themselves or, in a more general case, elements able to influence the dynamic balance between the subsystems. For this reason it is important to perform a good evaluation of the joint characteristics to obtain a good prediction of the system response. Unfortunately, it is difficult to define the mechanical parameters of the junctions and it is often affected by uncertainties.

A classical way to impose the uncertainties in the mathematical model is to consider random variable coefficients. When the randomness is a property of the lumped parameters of the structure the perturbation technique is one of the most valid methods [11,12].

Alternative to the random approach, two main methods have been recently exploited for the analysis of uncertain mechanical systems modelled with a finite element approach: the fuzzy and the interval approach [13–16].

The main reasons for studying new methodologies are that the classical random techniques, e.g. the Monte Carlo method, require a considerable computational effort, while the perturbation approaches are computationally efficient but cannot be used for large uncertainties and the estimation of the results depends on the "a priori" assumed probability distributions of each random variable. For these reasons it is useful to provide solutions that can give alternative and comparable uncertainty estimates.

A critical review of the so-called non-probabilistic methods can be found in Ref. [16], where it is clear that the fuzzy approach is not computationally economical although it is able to provide the whole fuzzy distribution of the solution uncertainty. On the other hand, the interval analysis approach, applied to mechanical problems, is considered computationally convenient because it produces the result in a single step of analysis. It gives as a result the limit bounds of an interval that includes all the possible values of the mechanical solution. The main drawback of this method is the overbounding of the amount of uncertainty in the solution, if a standard interval computational approach is used.

One part of the interval computations should hence be devoted to overcome the excess overbounding. Some authors have treated this subject in the structural mechanics framework. A perturbation approach can be used by calculating the first-order approximation of the dynamic equations. This method needs mathematical computation; it is very fast, but it does not guarantee the requirement of the inclusion of all the possible solutions. Another approach, derived from the Elishakoff anti-optimization, reduces the interval over-estimation by using ellipsoidal convex sets instead of intervals and it is used to estimate the worst case of the mechanical responses. Very recently a new technique based on affine analysis has been tested, and gives good results on uncertainty overbounding even if at a higher computational cost [17–20].

The goal of this paper is to study the effect of parametric uncertainties on the structural solution. This is a preliminary work in which attention is focused on the comparison between different techniques. The aim is to estimate whether one method is more appropriate than the others in determining a more reliable interval and in relation to computational burden. The studied test cases are simple to present a clear understanding of the effect of the uncertain parameters, a result that may not be achieved for complex systems. Therefore, the logic followed by the authors is to define the best technique to study structures with parametric uncertainties and to use this method to extend the conclusions reached to study, in next works, actual complex structures.

In particular, in this paper the random perturbation approach is compared with the interval approach, in which the uncertain parameters are defined by interval limits without any assumption on the whole uncertain distribution. Here, certain parameters are called crisp. In some reference works a comparison can be found between probabilistic and non-probabilistic approaches, either from a theoretical or from a computational point of view [21–23]. In fact, it is reported that the interval solutions generally include the probabilistic ones, and generally they are computationally advantageous. In this work the two approaches are compared with respect to the amount of final uncertainty by defining two proper uncertainty indices: one for the random perturbation case and one for the interval case. These indices can be directly compared. The interval equations of the problem are directly obtained by an interval algebraic method that can be simply applied to the energy

flow equations that, in this case, are expressed by rational functions. As mentioned, the main drawback of the standard interval approaches is solution overbounding [24,25]. To cope with this problem an alternative method is also presented. This method is based on a convergence theorem of the interval arithmetic. The evaluation of a rational function on a proper set of sub-intervals, rather than on its set union, and the union of this set of results guarantee the inclusion of all possible solutions on a narrower interval [24].

The developed interval equations are used to find the energy flow solution of three simple mechanical models; the best interval solutions are finally compared with the random solution.

2. Interval arithmetic

An uncertain interval quantity is represented here by an interval number $[x] = [x_{\inf}, x_{\sup}] = x_c + \Delta x\, e_\Delta$, where $x_{\inf}$ and $x_{\sup}$ are the "infimum" and "supremum" limits of the interval or $x_c = (x_{\inf} + x_{\sup})/2$ and $e_\Delta = [-1, 1]$ are the central value and the unit interval scaled by the radius $\Delta x = (x_{\sup} - x_{\inf})/2$, respectively. The first notation is more useful for computations, whereas the second notation is more expressive because it associates a crisp evaluation x_c with the amount of uncertainty Δx.

The notation used in the text is in italics for crisp numbers and square brackets enclose the letters that represent intervals with the previous settings.

The algebraic operations between intervals can be defined by crisp operations between the interval definition limits $x_{\inf}$ and $x_{\sup}$ [24]. For example the standard arithmetic is defined for the intervals $[x] = [a, b]$ and $[y] = [c, d]$ as

$$\begin{cases} [x] + [y] = [a + c, b + d], \\ -[y] = [-d, -c], \\ [x][y] = [\min\{ac, ad, bc, bd\}, \max\{ac, ad, bc, bd\}], \\ 1/[y] = \left[1/d, 1/c\right] \text{ and } [x]/[y] = [x]\left(1/[y]\right) \quad \text{if } 0 \notin [y]. \end{cases} \tag{1}$$

In general terms the result of an interval expression is the *inclusion* of all the possible values obtained when every variable varies *independently* within its limits. By applying this rule to the composition of standard operations, it follows that "the result of an interval expression is generally over-bounded and depends on the number of occurrences of the same variable in the expression". This aspect of interval computation is called "dependency" [25] and its effect is to widen the uncertainty of the result. An example of the dependency effect is given for $[x] = [1, 3]$ and $[y] = [1, 9]$:

$$\frac{[x]}{[x] + [y]} = [0.08, 1.50] \supset \frac{1}{1 + ([y]/[x])} = [0.10, 0.75], \tag{2}$$

where the results are directly obtained by applying the rules of Eq. (1). In the example, the true and narrower result is given by the second expression, in which intervals appear with a minimum number of occurrences. The result given by the left-hand expression is wider, but includes the true bounds. It should be noted that, since intervals are special kind of sets, both algebraic and set operations can be applied.

With respect to the present work, it is also useful to introduce the interval power computation rule:

$$[x]^n = \begin{cases} [1, 1], & n = 0, \\ [a^n, b^n], & a \geqslant 0 \text{ or } 0 \in [a, b] \text{ and } n \text{ is odd}, \\ [b^n, a^n], & b \leqslant 0, \\ [0, \max(a^n, b^n)], & 0 \in [c, d] \text{ and } n \text{ is even}. \end{cases} \tag{3}$$

By using the $[x]$ interval definition based on the central value x_c and interval radius Δx, as defined above, it is useful to introduce a comparison index for the solution that is called relative uncertainty and it is expressed as

$$\Delta_r = \frac{2\,\Delta x}{x_c}. \tag{4}$$

3. Inclusion and hull

Reliable results from interval computations are obtained if the true solutions are always included in the computed intervals, no matter how the computations are performed. For this reason the inclusion property needs to be verified and it is important to know the inclusion capability of the used functions or algorithms. In Moore's book [24], it is demonstrated that rational interval functions, i.e. functions whose computation follows the rules of Eqs. (1) and (3), include the true solution in a *monotonic* way. This means that, if an interval rational function $f([x])$ is evaluated in two intervals such that $[x_1] \supset [x_2]$, it is also true that $f([x_1]) \supset f([x_2])$. This is shown by the graphical example of Fig. 1, where the interval representation of the function $f([x]) = [x](1 - [x])$, evaluated at nested monotonic decreasing intervals, is compared with the crisp line that represents $f(x) = x(1 - x)$.

From this simple example an important observation can be drawn: as the radius Δx of $[x]$ decreases, the overbounding of $f([x])$ reduces correspondently. Therefore, as $\Delta x \to 0 [x] \to x_c$ and $f([x]) \to f(x_c)$.

From this first example it can be further shown how the hull of an interval function can be calculated by minimizing the overestimation due to interval computation.

In general, the inclusion range of a crisp function $R[f(x)]_X$ can be defined as the interval calculated by solving the optimization problems $[\min\{f(x)\}, \max\{f(x)\}]_X$ over a bounded domain X, with $x \in X$. From the interval point of view, $R[f(x)]_X$ can be calculated as the minimum inclusion interval $[Y] = f([x])$, with $[x] = X$, as the interval hull such that $R[f(x)]_X \subseteq [Y]$.

As mentioned in the case of interval rational functions, which are composed of the standard operations (1), the hull $[Y]$ is overestimated. To minimize the overestimation, the following theorem given in Moore's book [24] can be applied.

Supposing that $[x]$ is subdivided into disjoined sub-intervals $[x]_i$ such that:

$$[x] = \bigcup_i [x]_i \tag{5}$$

then the interval hull $[Y]$ can be included as

$$R[f(x)]_X \subseteq \bigcup_i f([x]_i) \subseteq [Y]. \tag{6}$$

A graphical example of theorem (6) is depicted in Fig. 2, where the interval hull ($[Y] = [-2, -1]$) of the function $f([x]) = [x]^2 + 2[x] - 1$ is bounded over the domain $X = [-2, 0]$ by applying Eq. (5) for different subdivisions of $[x] = X$.

4. Energy flow analysis

For the sake of generality let us consider two multi-degree-of-freedom (multi-dof) systems coupled by a massless non-conservative joint (Fig. 3). The system I is loaded by a harmonic force $f_1(t) = F_1 e^{j\omega t}$. The

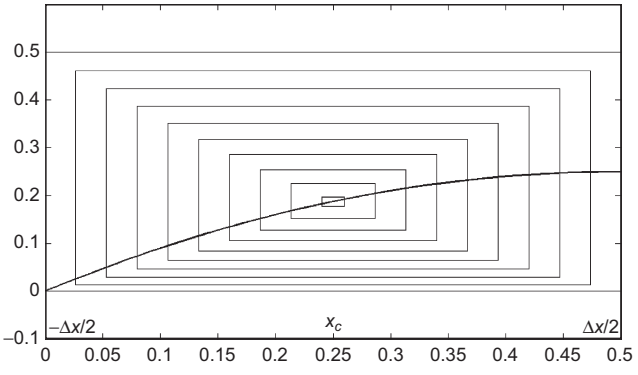

Fig. 1. Interval evaluation with monotonic convergence.

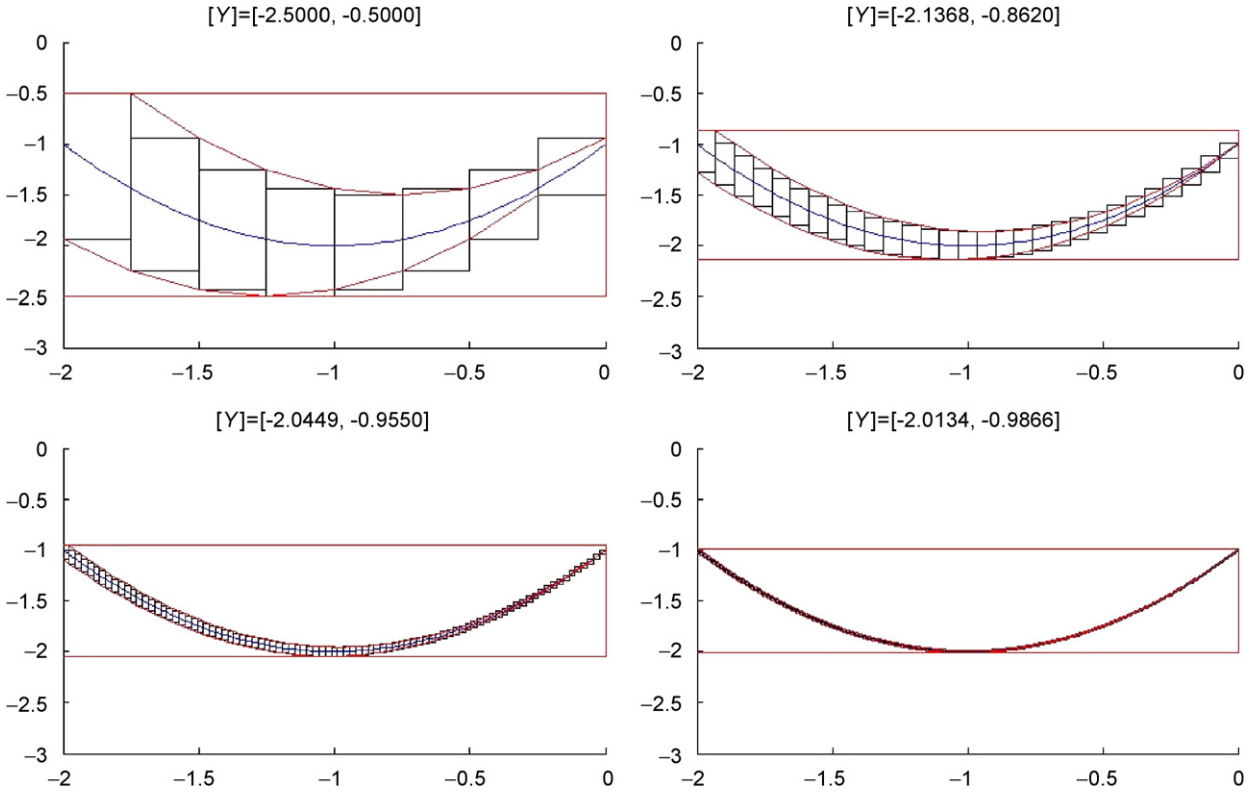

Fig. 2. Interval hull inclusion by different domain (X) subdivisions.

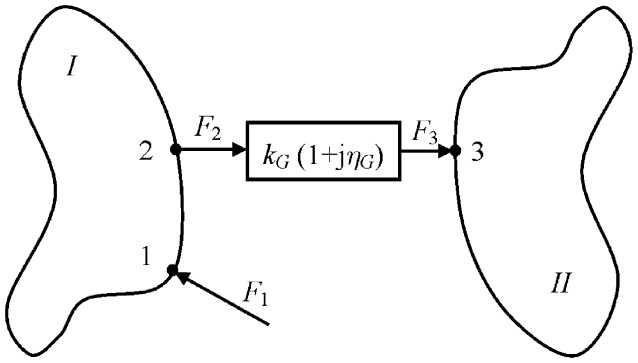

Fig. 3. The jointed multi-dof systems.

time-average power at each point of the systems is given by the following relationship:

$$P_i = \tfrac{1}{2}\mathrm{Re}\{F_i V_i^*\}, \tag{7}$$

where F_i and V_i are the phasors of the force and of the velocity at point i and * indicates a complex conjugate.

The following mobility equations can be written for systems I and II:

$$\begin{aligned} V_1 &= M_{11}F_1 - M_{12}F_2, \\ V_2 &= M_{21}F_1 - M_{22}F_2, \\ V_3 &= M_{33}F_3. \end{aligned} \tag{8}$$

Since the joint is massless, the following relationship holds:

$$F_2 = F_3 \tag{9}$$

and the next equation can be considered:

$$V_2 = F_2(M_{33} + M_{\mathrm{III}}). \tag{10}$$

The mobility of the joint (system III) is

$$M_{\mathrm{III}} = \frac{\omega(\eta_G + \mathrm{j})}{k_G(\eta_G^2 + 1)}, \tag{11}$$

when k_G and η_G are the stiffness and the damping of the joint, respectively.

The set of Eqs. (8)–(10) allows to write the following relationship for the powers at the points 2 and 3:

$$P_2 = \frac{1}{2}\frac{|M_{21}F_1|^2}{|M_{33} + M_{22} + M_{\mathrm{III}}|^2}\,\mathrm{Re}\,\{M_{33}^*\}, \tag{12}$$

$$P_3 = -\frac{1}{2}\frac{|M_{21}F_1|^2}{|M_{33} + M_{22} + M_{\mathrm{III}}|^2}\,\mathrm{Re}\,\{M_{33}^* + M_{\mathrm{III}}\}. \tag{13}$$

By considering Eq. (11) and assuming $\eta_G \ll 1$, the previous equations becomes

$$P_2 = \frac{1}{2}\frac{|M_{21}F_1|^2}{|M_{33} + M_{22} + \omega(\eta_G + \mathrm{j})/k_G|^2}\,\mathrm{Re}\,\{M_{33}^*\}, \tag{14}$$

$$P_3 = -\frac{1}{2}\frac{|M_{21}F_1|^2}{|M_{33} + M_{22} + \omega(\eta_G + \mathrm{j})/k_G|^2}\,\mathrm{Re}\,\{M_{33}^* + \omega(\eta_G + \mathrm{j})/k_G\}. \tag{15}$$

Since the uncertainties of the system are lumped in the joint, its parameters (k_G and η_G) are the uncertain coefficients of the problem. Therefore, Eqs. (14) and (15) can be rewritten by collecting these terms. The following relationships hold:

$$P_3 = \frac{A}{\alpha + 2\omega(a\eta_G + b)/k_G + \omega^2/k_G^2}, \tag{16}$$

$$P_2 = -P_3 - \frac{B\omega\eta_G/k_G}{\alpha + 2\omega(a\eta_G + b)/k_G + \omega^2/k_G^2}, \tag{17}$$

where

$$\begin{aligned} &B = \frac{1}{2}|M_{21}F_1|^2, \quad A = B\,\mathrm{Re}\,\{M_{33}^*\}, \\ &a = \mathrm{Re}\,\{M_{33}\} + \mathrm{Re}\,\{M_{22}\}, \quad b = \mathrm{Im}\,\{M_{33}\} + \mathrm{Im}\,\{M_{22}\}, \quad \alpha = a^2 + b^2. \end{aligned} \tag{18}$$

It is important to focus attention on the sign of each previous term. All the coefficients defined in Eq. (18) are positive except b. In fact, they are the absolute values or the real part of the point mobility. On the contrary, the sign of the imaginary part of the mobility changes, assuming positive or negative values [11].

5. Interval analysis of the energy flow

By assuming the expressions defined for P_2 and P_3 in the previous section and by applying the given rules of interval computations, the expressions of interval powers $[P_2]$ and $[P_3]$ can be found. By considering the interval parameters $[\eta_G]$ and $[k_G]$, $[P_3]$ can be written as follows:

$$[P_3] = \frac{A}{\alpha + 2\omega((a[\eta_G] + b)/k_G) + \omega^2(1/[k_G]^2)}. \tag{19}$$

By applying the interval arithmetic rules (1) and the interval power rule (3), the interval solution is found to be:

$$[P_3] = \frac{A}{[T]} = \left[\frac{A}{T_{\sup}}, \frac{A}{T_{\inf}}\right], \tag{20}$$

where

$$[T] = \alpha + 2\omega[T_2] + \omega^2[T_1] \tag{21}$$

with

$$[T_1] = \left[\frac{1}{k^2_{G,\sup}}, \frac{1}{k^2_{G,\inf}}\right],$$
$$[T_2] = \begin{cases} \left[\dfrac{a\eta_{G,\inf}+b}{k_{G,\sup}}, \dfrac{a\eta_{G,\sup}+b}{k_{G,\inf}}\right] & \text{if } a[\eta_G]+b>0, \\ \left[\dfrac{a\eta_{G,\inf}+b}{k_{G,\inf}}, \dfrac{a\eta_{G,\sup}+b}{k_{G,\sup}}\right] & \text{if } a[\eta_G]+b<0. \end{cases} \tag{22}$$

The solution given by Eq. (22) is found by supposing that $a[\eta_G]+b$ takes on positive or negative values alternatively for all the values within the interval $[\eta_G]$.

Likewise, the interval solution for $[P_2]$ can be found as

$$[P_2] = -[P_3] + B\omega\frac{[T_3]}{[T]} = \left[-\frac{A}{T_{\inf}} + B\omega\frac{T_{3,\inf}}{T_{\sup}}, -\frac{A}{T_{\sup}} + B\omega\frac{T_{3,\sup}}{T_{\inf}}\right] \tag{23}$$

with

$$[T_3] = -\frac{[\eta_G]}{[k_G]} = \left[-\frac{\eta_{G,\sup}}{k_{G,\inf}}, -\frac{\eta_{G,\inf}}{k_{G,\sup}}\right]. \tag{24}$$

6. Statistics of the energy flow

Let us consider a random variability of the joint parameters

$$k_G = k_{G0}(1+\varepsilon_1), \quad \eta_G = \eta_{G0}(1+\varepsilon_2), \tag{25}$$

where k_{G0} and η_{G0} are the reference deterministic values of the stiffness and damping, respectively, while ε_1 and ε_2 are dimensionless and zero mean random variables. They are uncorrelated.

In this paper a perturbation technique is shown to study the statistical moments of the energy flows. When ε_1 and ε_2 are small, a series expansion of P_2 and P_3 in the neighbourhood of the mean values can be written:

$$P_3 \simeq P_3|_0 + \left.\frac{\partial P_3}{\partial\varepsilon_1}\right|_0 \varepsilon_1 + \left.\frac{\partial P_3}{\partial\varepsilon_2}\right|_0 \varepsilon_2, \quad P_2 \simeq P_2|_0 + \left.\frac{\partial P_2}{\partial\varepsilon_1}\right|_0 \varepsilon_1 + \left.\frac{\partial P_2}{\partial\varepsilon_2}\right|_0 \varepsilon_2. \tag{26}$$

By substituting Eqs. (16) and (17) into Eq. (26), the following relationships provide the deterministic terms of the series:

$$P_3|_0 = \frac{Ak^2_{G0}}{\omega^2 + 2k_{G0}(b+a\eta_{G0})\omega + \alpha k^2_{G0}},$$
$$\left.\frac{\partial P_3}{\partial\varepsilon_1}\right|_0 = 2\frac{Ak^2_{G0}\omega^2 + Ak^3_{G0}(b+a\eta_{G0})\omega}{(\omega^2 + 2k_{G0}(b+a\eta_{G0})\omega + \alpha k^2_{G0})^2},$$
$$\left.\frac{\partial P_3}{\partial\varepsilon_2}\right|_0 = -2\frac{Ak^3_{G0}a\eta_{G0}\omega}{(\omega^2 + 2k_{G0}(b+a\eta_{G0})\omega + \alpha k^2_{G0})^2}, \tag{27}$$

$$P_2|_0 = -P_3|_0 - \frac{B\omega\eta_{G0}k_{G0}}{\omega^2 + 2k_{G0}(b + a\eta_{G0})\omega + \alpha k_{G0}^2},$$
$$\left.\frac{\partial P_2}{\partial \varepsilon_1}\right|_0 = -\left.\frac{\partial P_3}{\partial \varepsilon_1}\right|_0 - \frac{B\eta_{G0}k_{G0}\omega^3 - B\eta_{G0}\alpha k_{G0}^3\omega}{(\omega^2 + 2k_{G0}(b + a\eta_{G0})\omega + \alpha k_{G0}^2)^2},$$
$$\left.\frac{\partial P_2}{\partial \varepsilon_2}\right|_0 = -\left.\frac{\partial P_3}{\partial \varepsilon_2}\right|_0 - \frac{B\eta_{G0}k_{G0}\omega^3 + 2B\eta_{G0}k_{G0}^2 b\omega^2 + B\alpha\eta_{G0}k_{G0}^3\omega}{(\omega^2 + 2k_{G0}(b + a\eta_{G0})\omega + \alpha k_{G0}^2)^2}. \tag{28}$$

The first- and second-order statistical moments of P_2 and P_3 are, respectively,

$$E\{P_2\} \simeq P_2|_0, \quad E\{P_3\} \simeq P_3|_0 \tag{29}$$

and

$$E\{P_2^2\} \simeq P_2^2|_0 + \left(\left.\frac{\partial P_2}{\partial \varepsilon_1}\right|_0\right)^2 \sigma_{\varepsilon_1}^2 + \left(\left.\frac{\partial P_2}{\partial \varepsilon_2}\right|_0\right)^2 \sigma_{\varepsilon_2}^2,$$
$$E\{P_3^2\} \simeq P_3^2|_0 + \left(\left.\frac{\partial P_3}{\partial \varepsilon_1}\right|_0\right)^2 \sigma_{\varepsilon_1}^2 + \left(\left.\frac{\partial P_3}{\partial \varepsilon_2}\right|_0\right)^2 \sigma_{\varepsilon_2}^2. \tag{30}$$

Consequently, since the random variables ε_1 and ε_2 have mean void and are uncorrelated, the standard deviations are:

$$\sigma_{P_2} = \sqrt{\left(\left.\frac{\partial P_2}{\partial \varepsilon_1}\right|_0\right)^2 \sigma_{\varepsilon_1}^2 + \left(\left.\frac{\partial P_2}{\partial \varepsilon_2}\right|_0\right)^2 \sigma_{\varepsilon_2}^2}, \quad \sigma_{P_3} = \sqrt{\left(\left.\frac{\partial P_3}{\partial \varepsilon_1}\right|_0\right)^2 \sigma_{\varepsilon_1}^2 + \left(\left.\frac{\partial P_3}{\partial \varepsilon_2}\right|_0\right)^2 \sigma_{\varepsilon_2}^2}. \tag{31}$$

Therefore, the statistical moments of the energy flow depend linearly on the statistical moments of the same order of the random variables ε_1 and ε_2 [11].

The equations written in this section are valid for any probability density function (pdf).

Since the aim of this paper is to compare the results obtained by the standard interval analysis, the interval hull method and the stochastic perturbation technique, the dimensionless random variables are chosen with uniform pdf, because this distribution represents a closer choice to the interval description of the variable.

The following relationships hold for the first- and the second-order statistical moments and the standard deviation (std):

$$m_1 = \frac{x_2 + x_1}{2}, \quad m_2 = \frac{(x_2 - x_1)^2}{12}, \quad \sigma = \frac{x_2 - x_1}{2\sqrt{3}}. \tag{32}$$

A dimensionless coefficient, called the confidence factor here, is presented and defined as the ratio between the interval around the mean and the mean of the energy flow. By considering Eqs. (31) and (32), the following relationship holds:

$$f_{cP_i} \simeq \frac{2\sqrt{3}\sqrt{((\partial P_i/\partial \varepsilon_1)|_0)^2 \sigma_{\varepsilon_1}^2 + ((\partial P_i/\partial \varepsilon_2)|_0)^2 \sigma_{\varepsilon_2}^2}}{P_i|_0}, \quad i = 1, 2. \tag{33}$$

These coefficients can be compared with the relative uncertainty (4) to study the similarity between the interval and the random analysis.

7. Numerical results

Three systems are studied. The first one is a two-degrees-of-freedom (2-dof) oscillator jointed to another 2-dof oscillator (Fig. 4). The second one consists of two bending simply supported beams, coupled together by a non-conservative massless joint (Fig. 5). The third one is similar to the second one where the systems are two simply supported rectangular bending plates (Fig. 6).

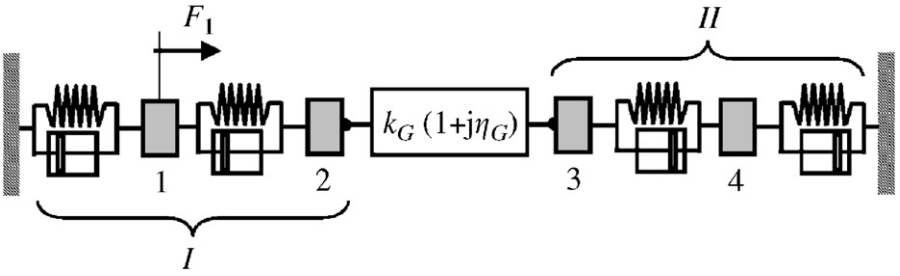

Fig. 4. The 2-dof–uncertain joint–2-dof system.

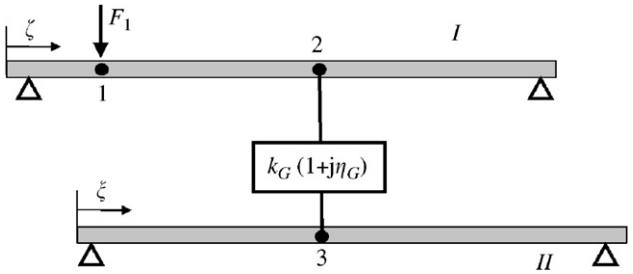

Fig. 5. The beam–uncertain joint–beam.

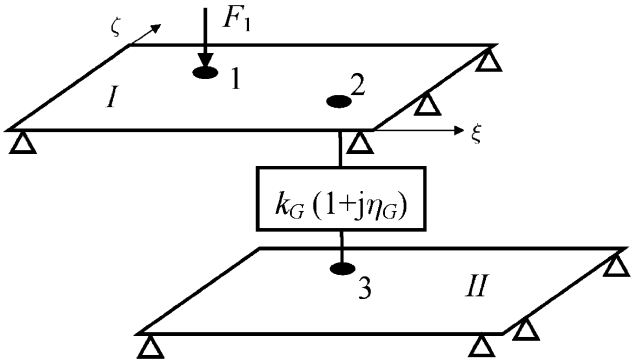

Fig. 6. The plate–uncertain joint–plate.

7.1. 2-dof oscillator– uncertain joint– 2-dof oscillator

The 2-dof oscillator is a two mass-spring-damper. Two 2-dof oscillators coupled together by a non-conservative massless joint (Fig. 4) are the first studied system.

The mobilities M_{21}, M_{22} and M_{33} can be calculated by the following equations:

$$\begin{bmatrix} M_{11} & M_{12} \\ M_{21} & M_{22} \end{bmatrix} = \frac{1}{\mathrm{j}\omega} \begin{bmatrix} -\omega^2 m_1 + \mathrm{j}\omega(c_1 + c_2) + k_1 + k_2 & -\mathrm{j}\omega c_2 + k_2 \\ -\mathrm{j}\omega c_2 + k_2 & -\omega^2 m_2 + \mathrm{j}\omega c_2 + k_2 \end{bmatrix}^{-1},$$

$$\begin{bmatrix} M_{33} & M_{34} \\ M_{43} & M_{44} \end{bmatrix} = \frac{1}{\mathrm{j}\omega} \begin{bmatrix} -\omega^2 m_3 + \mathrm{j}\omega c_3 + k_3 & -\mathrm{j}\omega c_3 + k_3 \\ -\mathrm{j}\omega c_3 + k_3 & -\omega^2 m_4 + \mathrm{j}\omega(c_4 + c_3) + k_4 + k_3 \end{bmatrix}^{-1}. \quad (34)$$

This test is contemporarily simple and general: four different test cases are investigated, with different values of the system parameters and joint parameters. The force always excites the point 1 and has 1.0 N

Table 1
The springs stiffness of the 2dof–uncertain joint–2dof system

	k_1 (N m^{-1})	k_2 (N m^{-1})	k_{G0} (N m^{-1})	k_3 (N m^{-1})	k_4 (N m^{-1})
$k_1,k_2<k_{G0}<k_3,k_4$	1000	1800	2500	3600	4000
$k_1,k_2>k_{G0}>k_3,k_4$	3600	4000	2500	1000	1800
$k_1,k_2<k_{G0}>k_3,k_4$	1000	1800	5500	3600	4000
$k_1,k_2>k_{G0}<k_3,k_4$	1000	1800	500	2000	1500

Table 2
Physical parameters of the two beams

	E (Pa)	ρ (kg m^{-3})	S (m^2)	L (m)	$\mathscr{I}$ (m^4)	η
First beam	2.1×10^{11}	7800	2×10^{-4}	1.5	1.6×10^{-9}	0.01
Second beam	2.1×10^{11}	7800	3×10^{-4}	2.5	2.5×10^{-9}	0.01

amplitude, while the stiffness of the springs changes for each different case and is chosen by the scheme in Table 1.

The mass and the damping values are, respectively, $m_1 = 1.0\,\mathrm{kg}$, $m_2 = 2.0\,\mathrm{kg}$, $m_3 = 1.5\,\mathrm{kg}$, $m_4 = 3.0\,\mathrm{kg}$, $c_1 = 0.1\,\mathrm{N\,s\,m^{-1}}$, $c_2 = 0.08\,\mathrm{N\,s\,m^{-1}}$, $c_3 = 0.07\,\mathrm{N\,s\,m^{-1}}$, and $c_4 = 0.04\,\mathrm{N\,s\,m^{-1}}$. The reference value of the joint damping is: $\eta_{G0} = 0.03$.

7.2. Beam–uncertain joint–beam

Two transversely vibrating supported beams are coupled together through a non-conservative joint as shown in Fig. 5.

The mobilities appearing in Eqs. (14) and (15) are given by the following relationships:

$$M_{21} = \frac{2\omega}{\rho_{\mathrm{I}} L_{\mathrm{I}} S_{\mathrm{I}}} \sum_n \frac{\varphi_{\mathrm{I}n}(\zeta_1)\varphi_{\mathrm{I}n}(\zeta_2)}{\eta_{\mathrm{I}}\omega_{\mathrm{I}n}^2 + \mathrm{j}(\omega^2 - \omega_{\mathrm{I}n}^2)},$$

$$M_{22} = \frac{2\omega}{\rho_{\mathrm{I}} L_{\mathrm{I}} S_{\mathrm{I}}} \sum_n \frac{\varphi_{In}(\zeta_2)^2}{\eta_{\mathrm{I}}\omega_{\mathrm{I}n}^2 + \mathrm{j}(\omega^2 - \omega_{\mathrm{I}n}^2)},$$

$$M_{33} = \frac{2\omega}{\rho_{\mathrm{II}} L_{\mathrm{II}} S_{\mathrm{II}}} \sum_n \frac{\varphi_{\mathrm{II}nm}(\xi_3)^2}{\eta_{\mathrm{II}}\omega_{\mathrm{II}n}^2 + \mathrm{j}(\omega^2 - \omega_{\mathrm{II}n}^2)}. \tag{35}$$

Eigenfunctions and natural frequencies are, respectively,

$$\varphi_n(\zeta) = sin\left(\frac{n\pi\zeta}{L}\right), \quad \omega_n = \left(\frac{n\pi}{L}\right)^2 \sqrt{\frac{E\mathscr{I}}{\rho S}}, \tag{36}$$

where E is the material Young modulus, ρ the material density, $\mathscr{I}$ the section second moment of area and S the area of the cross section. In Table 2 the values of the physical parameters used in the numerical test are reported.

The "Beam I" is loaded by a point force acting at $\zeta_1 = 0.3\,m$ and its amplitude is 1 N. The joint links the point $\zeta_2 = 0.7\,m$ of the first beam with the point $\xi_3 = 0.4\,m$ of the second one. Two tests are performed with this model: one when the reference stiffness of the joint is $k_{G0} = 1000\,\mathrm{N\,m^{-1}}$ and the reference damping is $\eta_{G0} = 0.01$, and the second when the reference damping is equal to that of the first test, while the reference stiffness of the joint is $k_{G0} = 10,000\,\mathrm{N\,m^{-1}}$.

Table 3
Physical parameters of the two plates

	E (Pa)	ρ (kg m^{-3})	ν	L_ζ (m)	L_ξ (m)	h (m)	η
First plate	2.1×10^{11}	7800	0.28	1	1.2	0.002	0.01
Second plate	2.1×10^{11}	7800	0.28	1.5	1.6	0.0025	0.01

7.3. Plate–uncertain joint–plate

Two bending rectangular plates simply supported along the four edges and coupled together by a non-conservative joint (Fig. 6) are the third studied case.

The mobilities are determined by

$$M_{21}=\frac{4\omega}{\rho_{\mathrm{I}}h_{\mathrm{I}}S_{\mathrm{I}}}\sum_{n,m}\frac{\varphi_{\mathrm{I}nm}(\zeta_1,\xi_1)\varphi_{\mathrm{I}nm}(\zeta_2,\xi_2)}{\eta_{\mathrm{I}}\omega_{\mathrm{I}nm}^2+\mathrm{j}(\omega^2-\omega_{\mathrm{I}nm}^2)},$$

$$M_{22}=\frac{4\omega}{\rho_{\mathrm{I}}h_{\mathrm{I}}S_{\mathrm{I}}}\sum_{n,m}\frac{\varphi_{\mathrm{I}nm}(\zeta_2,\xi_2)^2}{\eta_{\mathrm{I}}\omega_{\mathrm{I}nm}^2+\mathrm{j}(\omega^2-\omega_{\mathrm{I}nm}^2)},$$

$$M_{33}=\frac{4\omega}{\rho_{\mathrm{II}}h_{\mathrm{II}}S_{\mathrm{II}}}\sum_{n,m}\frac{\varphi_{\mathrm{II}nm}(\zeta_3,\xi_3)^2}{\eta_{\mathrm{II}}\omega_{\mathrm{II}nm}^2+\mathrm{j}(\omega^2-\omega_{\mathrm{II}nm}^2)}, \tag{37}$$

where S, h, ρ and η are the surface area, the thickness, the material density and the damping of each plate, respectively, while φ_{nm} and ω_{nm} are the eigenfunctions and the natural frequencies of the systems:

$$\varphi_{nm}(\zeta,\xi)=\sin\left(\frac{n\pi\zeta}{L_\zeta}\right)\sin\left(\frac{m\pi\xi}{L_\xi}\right),\quad \omega_n=\left[\left(\frac{n\pi}{L_\zeta}\right)^2+\left(\frac{m\pi}{L_\xi}\right)^2\right]\sqrt{\frac{Eh^2}{12\rho(1-\nu^2)}}. \tag{38}$$

In Table 3 the values of the physical parameters used in this numerical test are reported.

The first plate is excited by a force, $F_1=1.0\,N$, in ($\zeta_1=0.1\,\mathrm{m}$, $\xi_1=0.15\,\mathrm{m}$). The plates are connected at the points: ($\zeta_2=0.45\,\mathrm{m}$, $\xi_2=0.3\,\mathrm{m}$) on the first plate and ($\zeta_3=0.23\,\mathrm{m}$, $\xi_3=0.34\,\mathrm{m}$) on the second one.

As for the two beams test, also here two cases are investigated: $k_{G0}=1000\,\mathrm{N\,m^{-1}}$ and $\eta_{G0}=0.01$ are the joint parameters of the first one, while $k_{G0}=10,000\,\mathrm{N\,m^{-1}}$ and $\eta_{G0}=0.01$ are those of the second one.

8. Comments of the results

The systems are studied for $\varepsilon_1\in[-0.1,0.1]$ and $\varepsilon_2\in[-0.5,0.5]$. The interval around the mean is large and the efficiency of the perturbation method is strained.

Two comparisons are made for each vibrating system: the first is between the standard interval analysis and the interval hull method given by Eq. (6), and the second between the interval technique and the random perturbation technique. The stochastic results are obtained by summing the quantities $\pm\sqrt{3}\sigma$ to the mean value. Thus, the mean is compared with the interval central value and the supremum/infimum values of the interval are compared with the random interval extremes.

Fig. 7 show the change of the relative uncertainties mean with the number of subdivisions for the first test case of the "2-dof–uncertain joint–2-dof" (see Table 1). An average of the relative uncertainties is derived on the whole frequency range. The relative uncertainties decrease rapidly with the increment of subdivisions and tends to an asymptotic value.

Fig. 8 shows a detail of the energy flow P_2 spectrum. The nominal result is traced together with the inferior and the superior result provided by different techniques. These boundaries represent the uncertainty of the solution around the nominal value at each frequency. The results of the interval standard method and of the interval hull method are compared. As the number of sub-intervals increases (the bold arrows indicate the

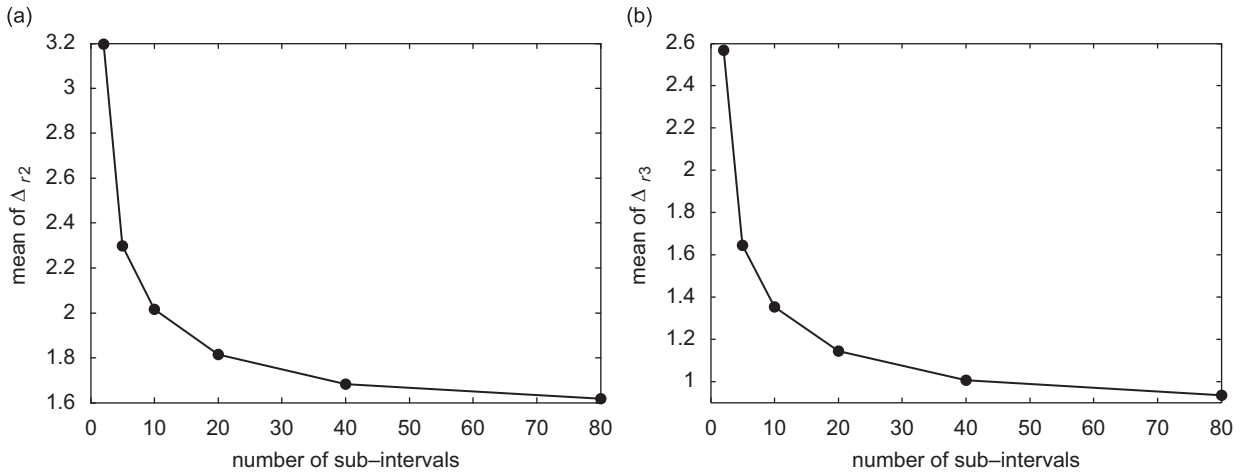

Fig. 7. 2-dof–uncertain joint–2-dof first test case: (a) P_2 relative uncertainty mean variation with the number of sub-intervals and (b) P_3 relative uncertainty mean variation with the number of sub-intervals.

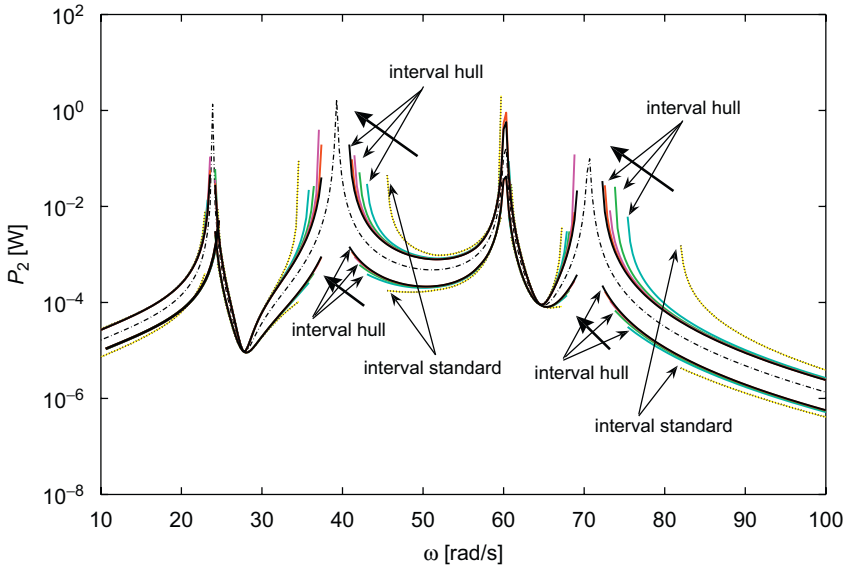

Fig. 8. P_2 of 2-dof–uncertain joint–2-dof first test case, interval standard vs. interval hull: variation of the sub-intervals number in a meaningful frequency band: (-.-.-.-.-.-.-.-.-.-) nominal solution; (……) interval standard technique solution (inferior and superior); and (_____) interval hull technique (inferior and superior, the subinterval numbers increase as the grey tone).

increase of the sub-intervals) the solution of the interval hull technique (grey-scale continuous lines) tends to a solution with a minimum uncertainty radius (black continuous line). To be more precise: the relative uncertainty decreases. It is shown that the result of the interval standard method gives the largest overestimation. In the frequency range close to the resonance peaks the interval solutions are not drawn because they rapidly tend to infinity. In fact, the solution is calculated by the classical interval operation defined in Eq. (1). The division is not defined if zero is included in the interval of the denominator and in this case the result is the interval $[-\infty, +\infty]$. In the studied case Eqs. (20) and (23) show the variable $[T]$ at the denominator. It can take on positive and negative values, so that T can be equal to zero. When this occurs the result is $[-\infty, +\infty]$ and Fig. 8 shows this behaviour at the resonance.

It is interesting to underline that the frequency range in which the interval solutions are not defined, and then not drawn, gives a measure of the resonances' uncertainty occurrence. In fact, since the inclusion is

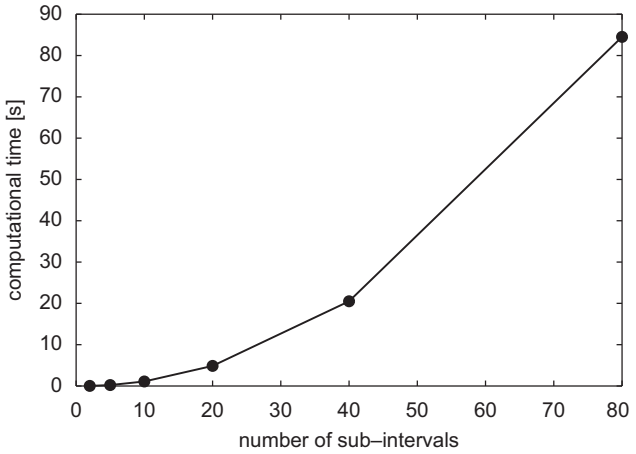

Fig. 9. 2-dof–uncertain joint–2-dof first test case: computational time variation with the number of sub-intervals.

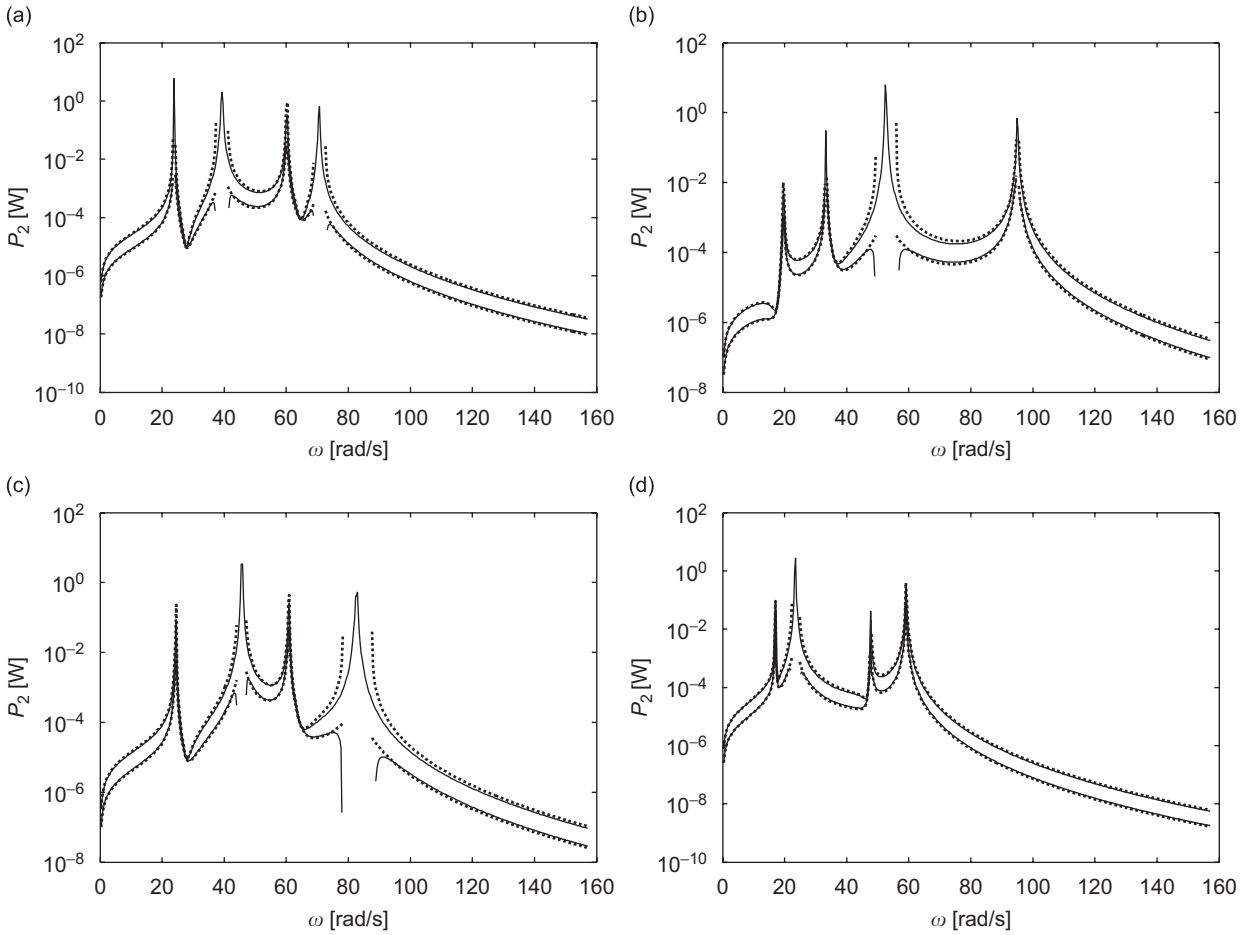

Fig. 10. P_2 of 2-dof–uncertain joint–2-dof: random (_____) vs. interval hull (…….): (a) first test case; (b) second test case; (c) third test case; and (d) fourth test case.

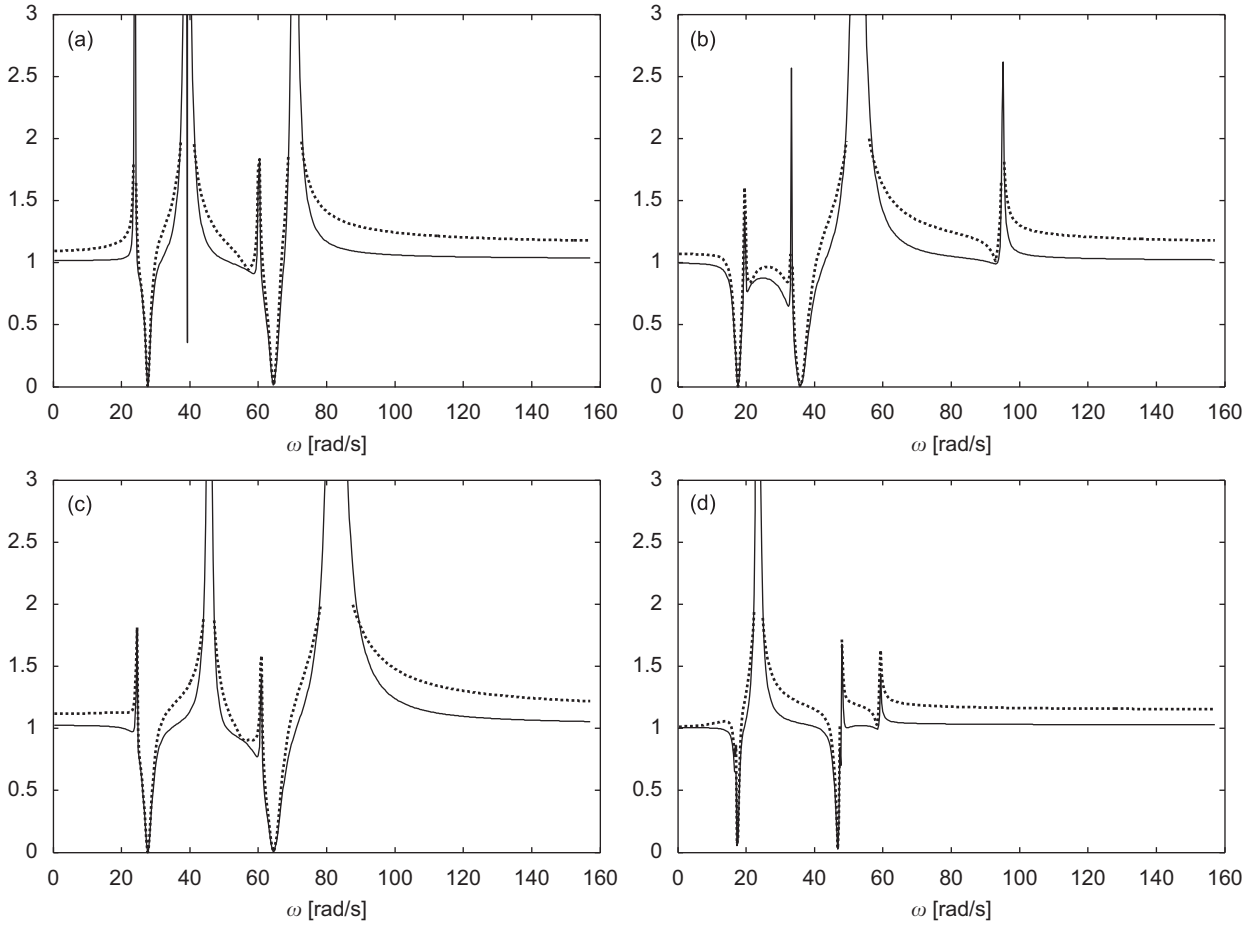

Fig. 11. 2-dof–uncertain joint–2-dof: P_2 confidence factor (_____) vs. relative uncertainty (……): (a) first test case; (b) second test case; (c) third test case; and (d) fourth test case.

guaranteed for each value of k_G and η_G chosen in their definition interval, the solution curves have a resonance in the frequency interval indicated in Fig. 8.

As the relative uncertainty decreases, the computational time increases (Fig. 9), because it is necessary to evaluate the solution for each subinterval. This technique does not reach the computational critical time of the Monte Carlo simulation, but if a large number of short sub-intervals is used the decrease of the response uncertainty is paid by an increase of the computational time. A good compromise, for this test case, between short times and close boundaries is 40 sub-intervals: the computational time is acceptable and the relative uncertainty is close to its asymptotic value, as shown in Figs. 7 and 9.

Fig. 10 shows the comparison between the best interval result (interval hull with 40 sub-intervals) and the random solution of P_2 spectrum for the four "2-dof–uncertain joint–2-dof" test cases shown in Table 1. Figs. 11 and 12 show the comparison between the relative uncertainties and the confidence factors.

To emphasize the difference between the two drawn curves, an appropriate y scale is chosen. The peaks of the confidence factors are cut, because their parts, which cannot be compared with the relative uncertainties, are not significant in this analysis. Unless around the natural frequencies a good agreement is found between the probabilistic and the interval results. Since the relative uncertainties and the confidence factors are defined to increase with an increase of uncertainty, at the resonance frequency they tend to infinity. In fact, as shown in Figs. 8 and 10, the uncertainty increases in the neighbourhood of the resonance.

The high-frequency behaviour of the relative uncertainties is meaningless in this set of test cases. In fact, this system has only four natural frequencies and at high-frequency values it does not show resonant behaviour.

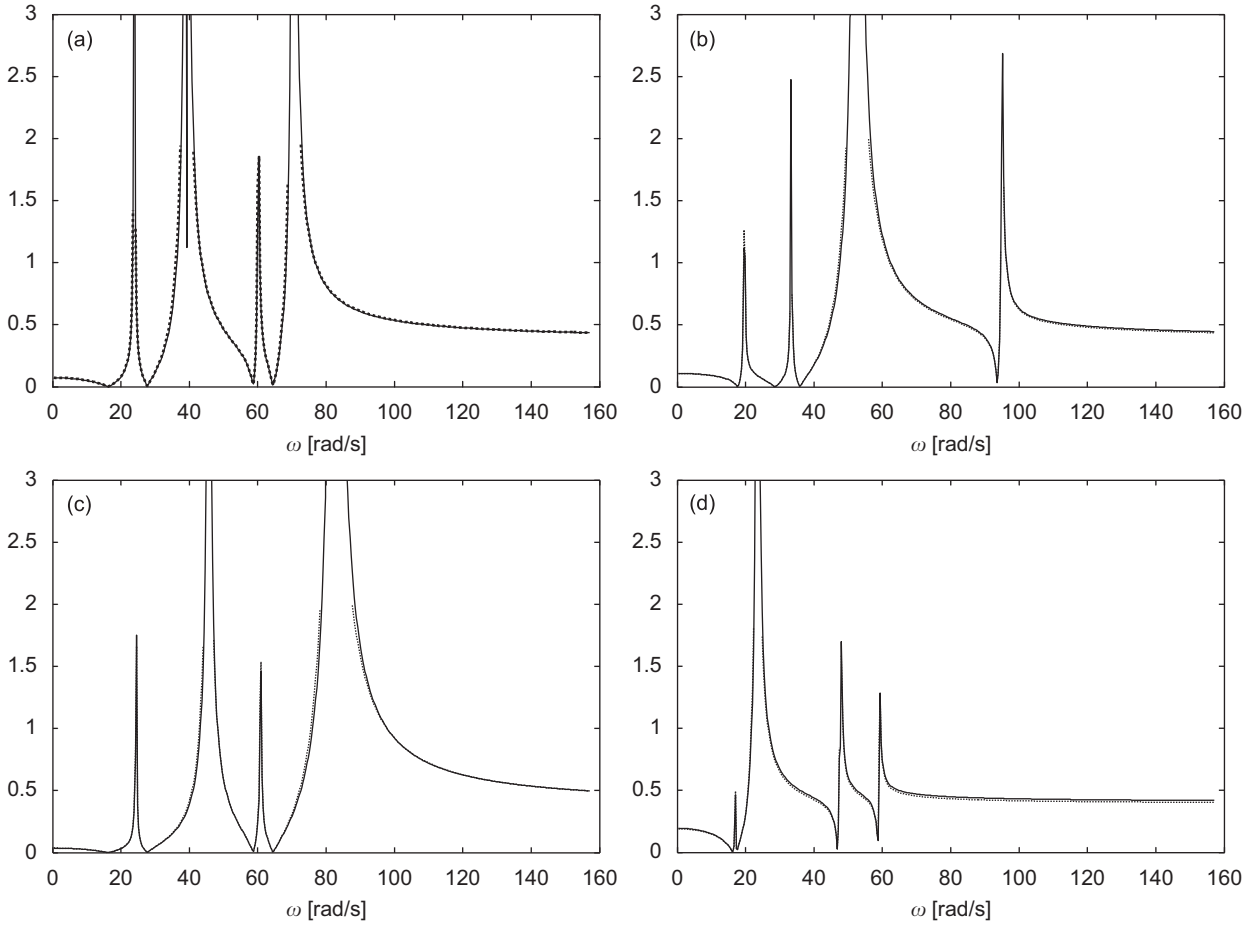

Fig. 12. 2-dof–uncertain joint–2-dof: P_3 confidence factor (_____) vs. relative uncertainty (……): (a) first test case; (b) second test case; (c) third test case; and (d) fourth test case.

The confidence factors and the relative uncertainties show an asymptotic behaviour in the frequency range away from the resonances. The gap between these two variables becomes constant and very similar for each test condition when the asymptotic behaviour occurs.

It is interesting to observe that the largest differences between the probabilistic and the interval solutions are found for the P_2 energy flow, while the confidence factor and the relative uncertainty of P_3 have a better agreement (Figs. 11 and 12). Moreover, Fig. 10 shows that the largest differences between the random and the interval methods are found when the joint has a nominal stiffness value close to the stiffness of the system springs. In fact, Fig. 10d, which represents the results for a weak coupling (see Table 1), shows the lowest difference. Equally, Figs. 11d and 12d show the lowest uncertainties.

The results of the two coupled beams system are investigated below.

Fig. 13 are similar to Fig. 7 and show the change of the mean of the relative uncertainties when $k_{G0} = 1000\,\mathrm{N\,m^{-1}}$. The computational time increases with the number of sub-intervals, as shown in Fig. 14. In this case the increment amount is higher than that seen for the discrete system.

A comparison between the interval standard and the interval hull results for P_2 is shown in Fig. 15.

At low frequencies, the interval hull method improves the solution. In fact, the interval around the nominal solution is smaller than the interval given by the standard interval computation (see Fig. 15a). Moreover, the graphics show that the interval hull guarantees solution inclusion also at the resonance frequencies where the result is more sensitive. Also in this case, at the resonance frequencies the curves of Fig. 15a show a jump. The reason is the same as that described before for the ''2-dof–uncertain joint–2-dof''.

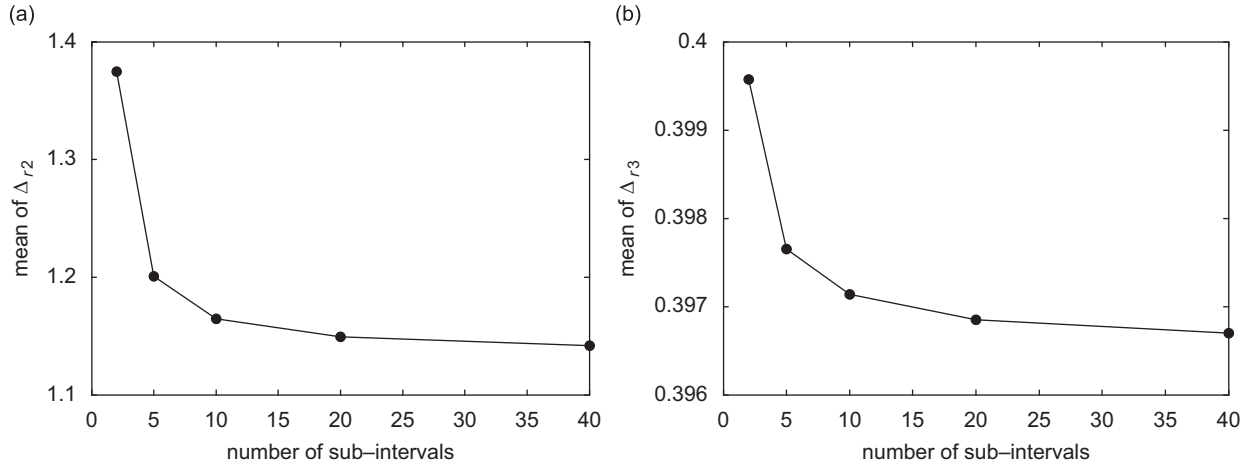

Fig. 13. Beam–uncertain joint–beam for $k_{G0} = 1000\,\mathrm{N\,m^{-1}}$: (a) P_2 relative uncertainty mean variation with the number of sub-intervals and (b) P_3 relative uncertainty mean variation with the number of sub-intervals.

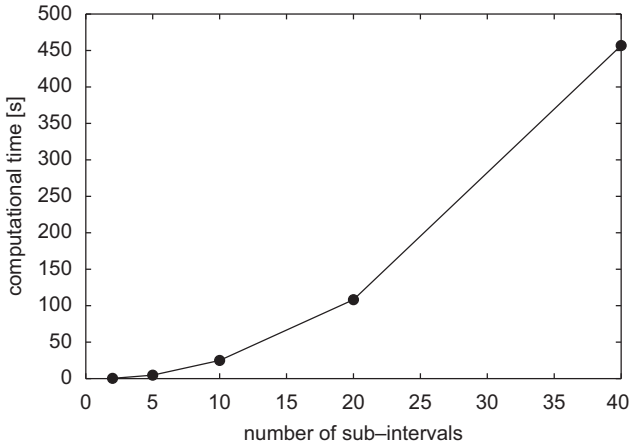

Fig. 14. Beam–uncertain joint–beam for $k_{G0} = 1000\,\mathrm{N\,m^{-1}}$: computational time variation with the number of sub-intervals.

At high frequencies the interval hull result is still better, but quite similar to that of the interval standard. This depends on the nature of the uncertain junction. In fact, the joint is localized and it is described as a point mobility. Therefore, it influences a few sets of modes of the coupled system.

In this frequency range the jump in correspondence of the eigenfrequencies does not occur, because the interval $[T]$ does not include the zero.

In Fig. 16 the confidence factors and the relative uncertainties of the energy flow P_2 and P_3, for $k_{G0} = 1000\,\mathrm{N\,m^{-1}}$, are compared. These two indices of the energy flow uncertainties have a good agreement and show an asymptotic similar behaviour to that at high frequencies. The high variation of these two variables at low-middle frequencies depends on the increase of uncertainties around the resonance frequencies. The sharper the resonance peaks, the higher the uncertainty at the eigenfrequencies. Moreover, as shown before in Fig. 15, the joint uncertainties affect the resonances in the frequency range [0–100] Hz more.

Fig. 17 shows the change of the mean of the relative uncertainties: on using the interval hull the sub-intervals increase. Fig. 18 shows a comparison between the confidence factors and the relative uncertainties of the energy flow P_2 and P_3 when $k_{G0} = 10,000\,\mathrm{N\,m^{-1}}$. The asymptotic behaviour of f_c and Δ_r is similar to that of the same variables for $k_{G0} = 1000\,\mathrm{N\,m^{-1}}$. On the contrary, at low frequencies the uncertainty around the resonance peaks is higher when k_{G0} is higher.

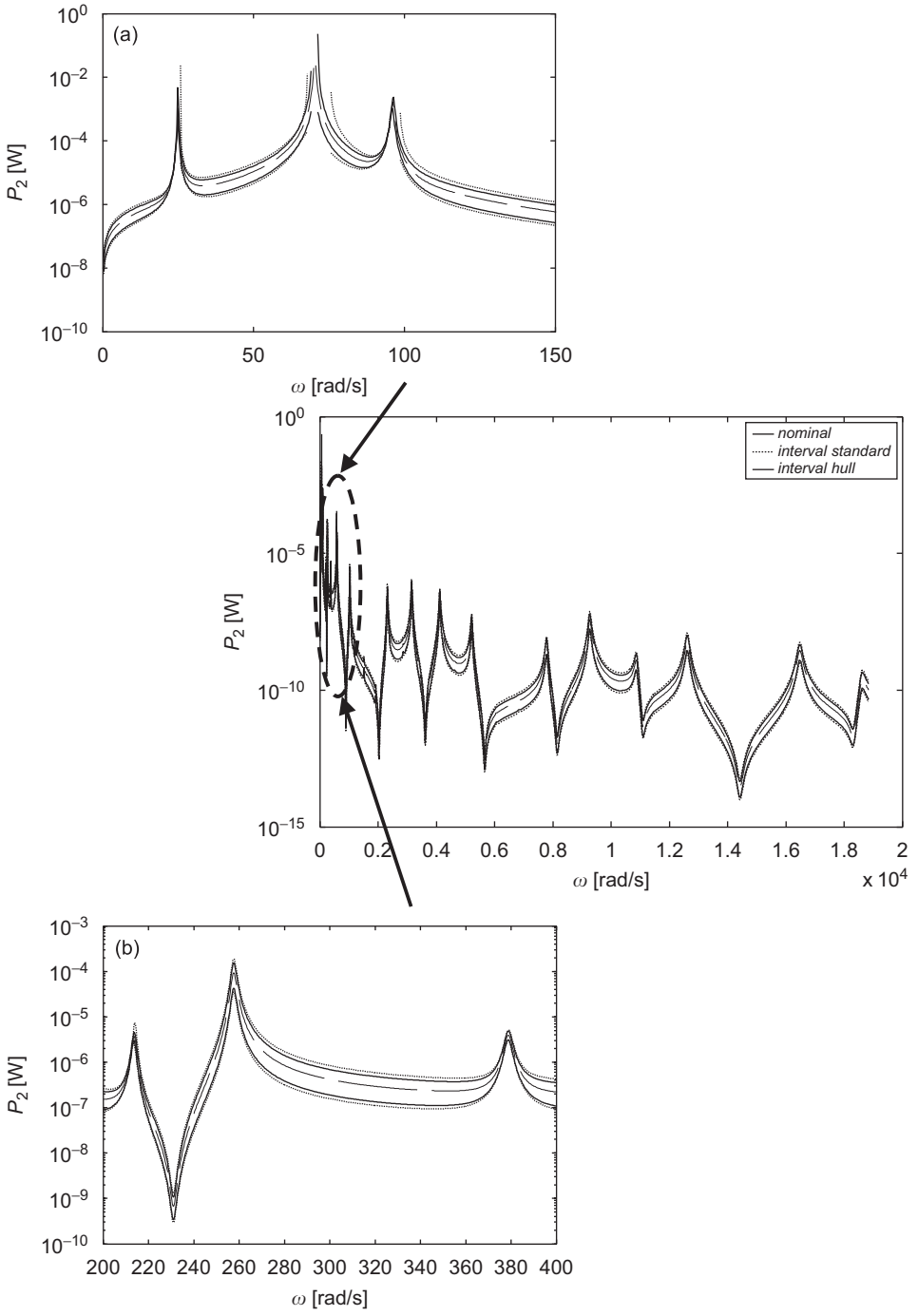

Fig. 15. P_2 of beam–uncertain joint–beam for $k_{G0} = 1000\,\mathrm{N\,m^{-1}}$, interval standard (……) vs. interval hull (_____): the whole studied frequency range and two zooms.

The results of the two plate systems are given in Figs. 19–22. Also, here, the increments of the sub-intervals improve the results of the interval hull (Figs. 19 and 21) up to convergence.

The comparison of the relative interval and the confidence factor (Figs. 20 and 22) shows, also in this case, a good agreement, especially for the energy flow P_3, and an asymptotic behaviour.

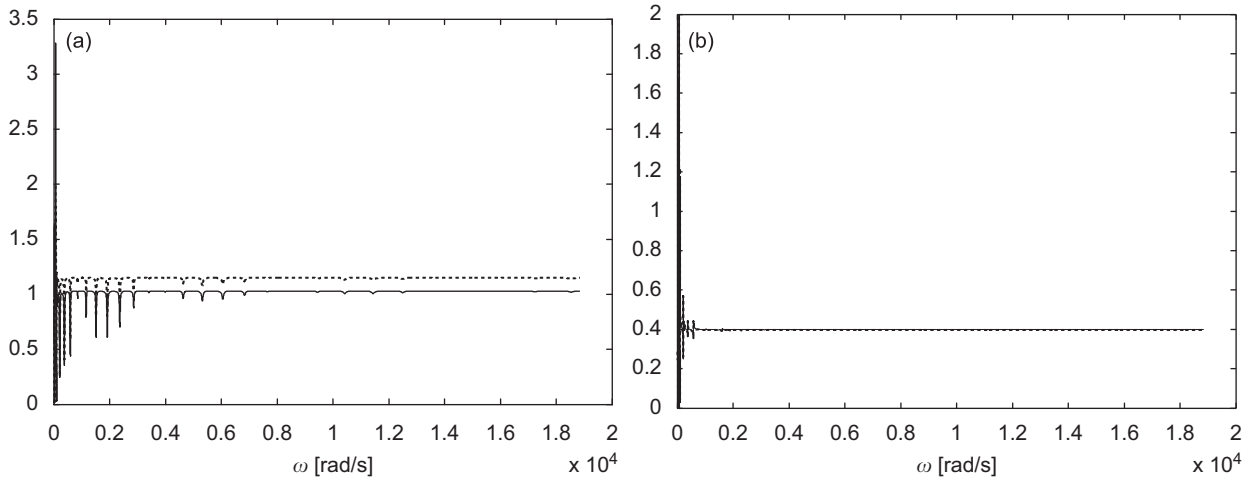

Fig. 16. Beam–uncertain joint–beam for $k_{G0} = 1000\,\mathrm{N\,m^{-1}}$: (a) P_2 confidence factor (_____) vs. relative uncertainty (……) and (b) P_3 confidence factor (_____) vs. relative uncertainty (……).

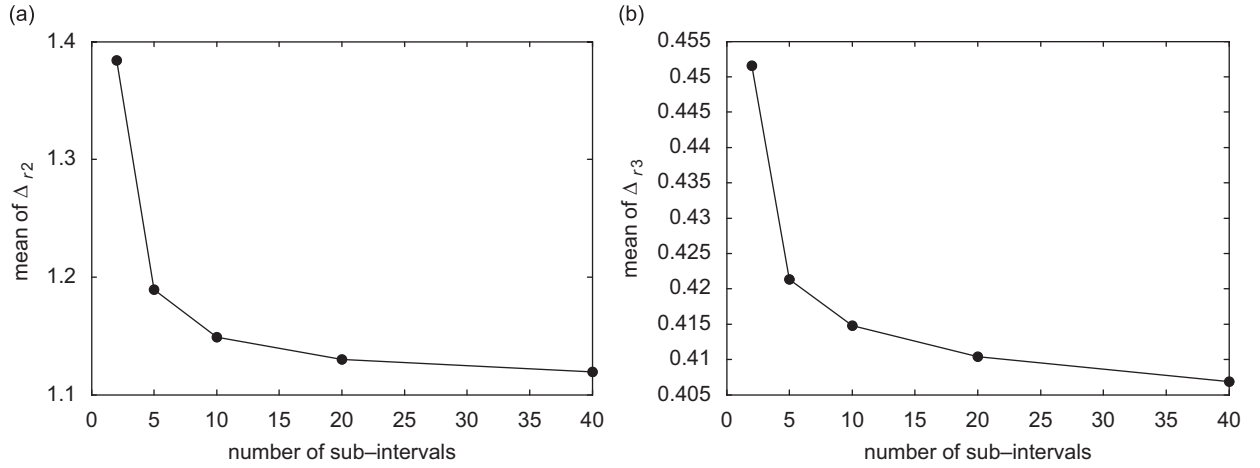

Fig. 17. Beam–uncertain joint–beam for $k_{G0} = 10,000\,\mathrm{N\,m^{-1}}$: (a) P_2 relative uncertainty mean variation with the number of sub-intervals and (b) P_3 relative uncertainty mean variation with the number of sub-intervals.

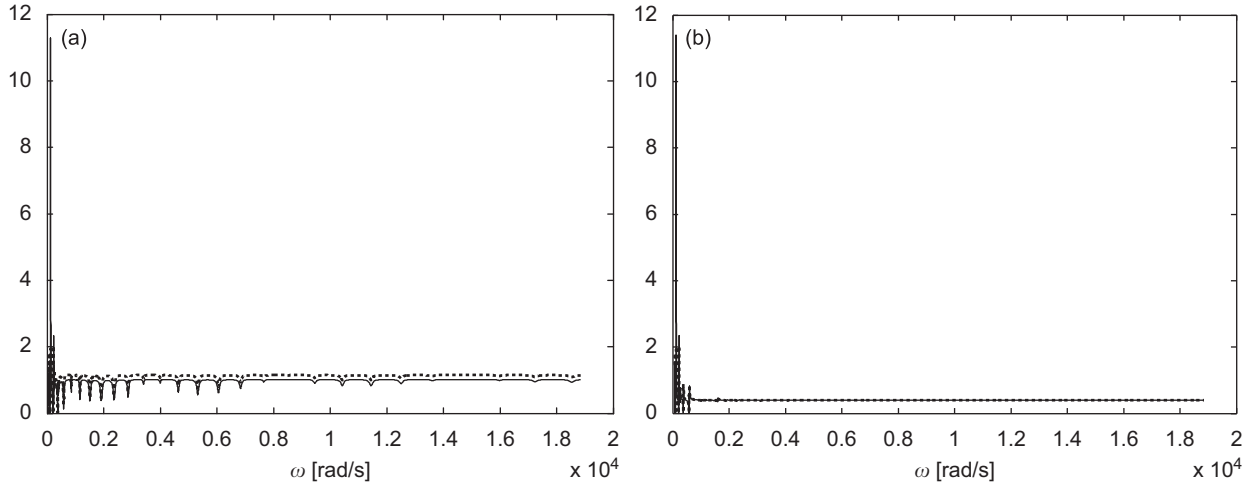

Fig. 18. Beam–uncertain joint–beam for $k_{G0} = 10,000\,\mathrm{N\,m^{-1}}$: (a) P_2 confidence factor (_____) vs. relative uncertainty (……) and (b) P_3 confidence factor (_____) vs. relative uncertainty (……).

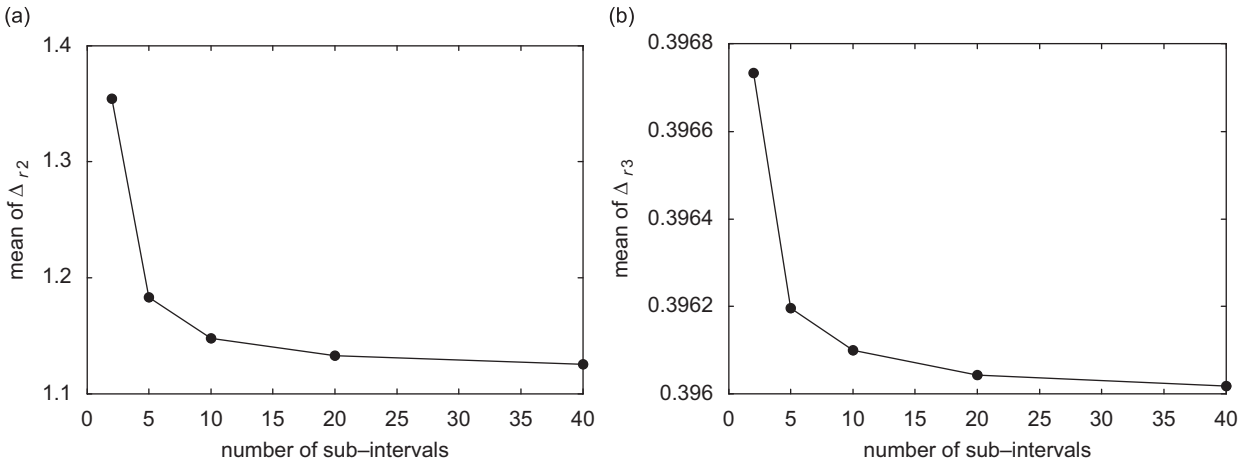

Fig. 19. Plate–uncertain joint–plate for $k_{G0} = 1000\,\mathrm{N\,m^{-1}}$: (a) P_2 relative uncertainty mean variation with the number of sub-intervals and (b) P_3 relative uncertainty mean variation with the number of sub-intervals.

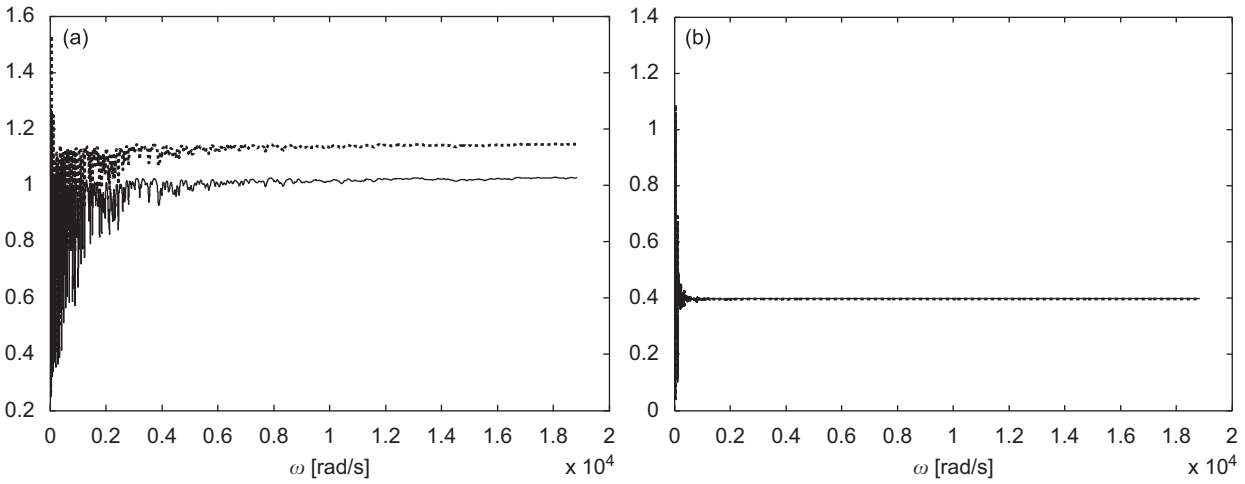

Fig. 20. Plate–uncertain joint–plate for $k_{G0} = 1000\,\mathrm{N\,m^{-1}}$: (a) P_2 confidence factor (_____) vs. relative uncertainty (…….) and (b) P_3 confidence factor (_____) vs. relative uncertainty (…….).

Since the modal density of the plates is higher than the modal density of the beams and the modal density of the plates is constant with frequency while that of the beams decreases, the graphics of f_c and Δ_r are more oscillating at low frequencies than those of the beams (Figs. 20 and 22).

9. Conclusions

The confidence of the energy flow level between three multimodal systems coupled by uncertain joints is studied using three different procedures: (i) the standard interval analysis, (ii) the interval hull analysis and (iii) a stochastic perturbation technique. The studied systems are simple, but general and consequently meaningful. One is discrete: "2-dof–uncertain joint–2-dof". Two are continuous: "beam–uncertain joint–beam" and "plate–uncertain joint–plate". The considered joint is a spring–damper system coupling one point of the first system with one point of the second one.

The results show that the best interval results are obtained by the interval hull technique which allows to improve the solution of the standard interval analysis by a slight increase of the computational time.

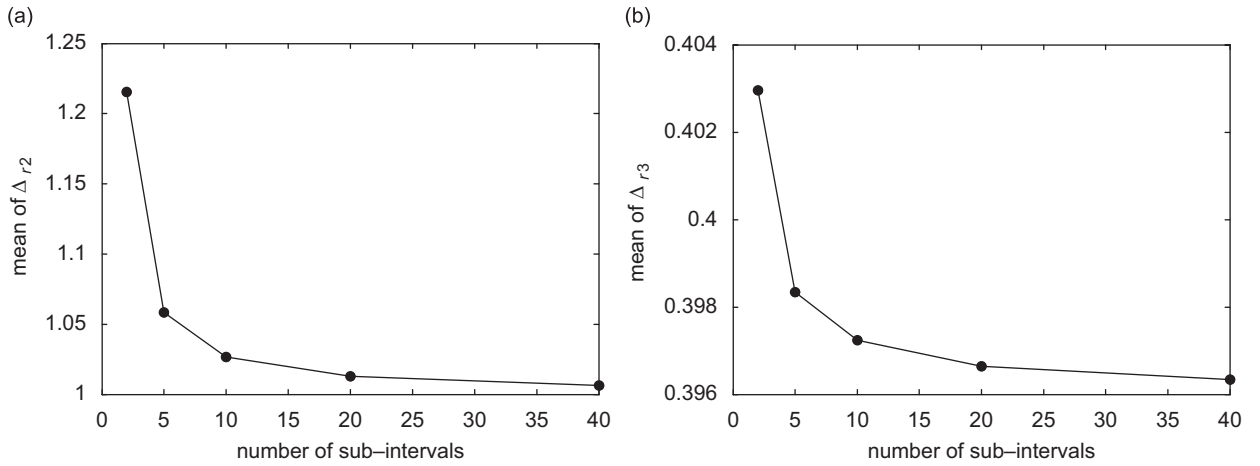

Fig. 21. Plate–uncertain joint–plate for $k_{G0} = 10,000\,\mathrm{N\,m^{-1}}$: (a) P_2 relative uncertainty mean variation with the number of sub-intervals and (b) P_3 relative uncertainty mean variation with the number of sub-intervals.

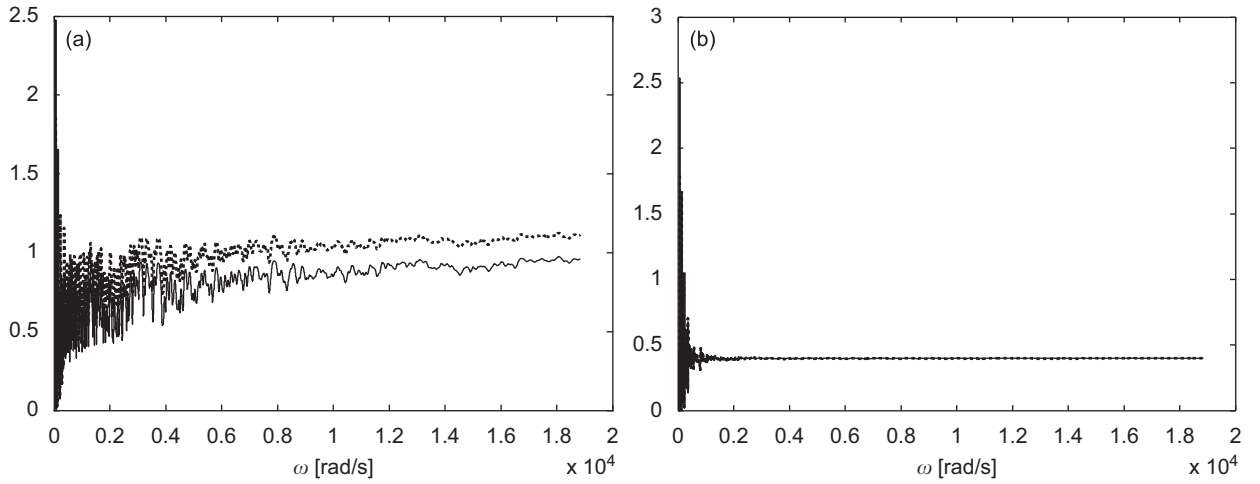

Fig. 22. Plate–uncertain joint–plate for $k_{G0} = 10,000\,\mathrm{N\,m^{-1}}$: (a) P_2 confidence factor (_____) vs. relative uncertainty (…….) and (b) P_3 confidence factor (_____) vs. relative uncertainty (…….).

Therefore, it is advisable to use this procedure always to obtain narrower interval uncertainty. A comparison of the results obtained using the interval hull and the probabilistic technique shows that very similar solutions are reached if the uncertainties are described by comparable laws and comparable characteristic parameters. In fact, in the studied cases a uniform pdf is used to describe the random uncertainty of the joint and the amplitude of the interval is chosen to be equal to the amplitude of the pdf. Therefore, the probabilistic and the interval methods are generally reversible.

In conclusion, the interval analysis is advantageous with respect to the probabilistic method studied in this paper, because: it does not require the knowledge of a probability distribution of the uncertainties, but only its interval bounds and, since it is not a perturbation technique, the interval analysis is not affected by the uncertainty of size.

In fact, when a parameter is considered uncertain, its value is effectively unknown in a bounded physical range. The assumption of a probability distribution in this range involves knowledge of the effective statistics of this parameter, that is generally an arbitrary assumption.

If the variance of the random variables is very high the stochastic perturbation technique fails and only a Monte Carlo method, with its computational burden, can provide a solution for the problem.

Moreover, when the number of uncertainty variables is small and analytical relationships can be written for the investigated physical quantities (e.g. energy flow), algebraic manipulations are sufficient to reach the equations that yield the interval solutions. On the contrary, more complicated mathematical computations are needed for the probabilistic approach.

References

[1] R.H. Lyon, On the vibration statistics of a randomly excited hard-spring oscillator, *The Journal of Acoustical Society of America* 32 (6) (1960) 716–719.
[2] H.G. Davies, Exact solutions for the response of some coupled multimodal systems, *The Journal of Acoustical Society of America* 51 (1B) (1972) 387–392.
[3] H.G. Davies, Power flow between two coupled beams, *The Journal of Acoustical Society of America* 51 (1B) (1972) 393–401.
[4] H.G. Davies, M.A. Wahab, Ensemble averages of power flow in randomly excited coupled beams, *Journal of Sound and Vibrations* 77 (3) (1981) 311–321.
[5] B.R. Mace, Power flow between two continuous one-dimensional subsystems: a wave solution, *Journal of Sound and Vibration* 154 (2) (1992) 289–319.
[6] F. Fahy, *Sound and Structural Vibration Radiation, Transmission and Response*, Academic Press, London, 1985.
[7] L. Cremer, M. Heckl, E.E. Ungar, *Structure-borne Sound*, second ed, Springer, Heidelberg, 1988.
[8] M.P. Norton, *Fundamentals of Noise and Vibration Analysis for Engineers*, Cambridge University Press, Cambridge, 1989.
[9] F. Fahy, Statistical energy analysis: a critical overview, in: A.J. Keane, W.G. Price (Eds.), *Statistical Energy Analysis*, Cambridge University Press, Cambridge, 1994.
[10] R.H. Lyon, R.G. De Jong, *Theory and Applications of Statistical Energy Analysis*, second ed, Butterworth-Heinemann, Boston, 1995.
[11] A. Culla, A. Sestieri, A. Carcaterra, Energy flow uncertainties in vibrating systems: definition of a statistical confidence factor, *Mechanical System and Signal Processing* 17 (3) (2003) 635–663.
[12] I. Elishakoff, *Probabilistic Theory of Structures*, second ed., Dover Publications, Inc., 1999.
[13] A.D. Dimarogonas, Interval analysis of vibrating systems, *Journal of Sound and Vibration* 183 (4) (1995) 739–749.
[14] O. Dessombz, F. Thouverez, J.P. Laîné, L. Jézéquel, Analysis of mechanical systems using interval computations applied to finite element methods, *Journal of Sound and Vibration* 239 (5) (2001) 949–968.
[15] D. Moens, A Non-probabilistic Finite Element Approach for Structural Dynamic Analysis with Uncertain Parameters, PhD Thesis, KU Leuven, 2002.
[16] D. Moens, D. Vandepitte, A survey of non-probabilistic uncertainty treatment in finite element analysis, *Computer Methods in Applied Mechanics and Engineering* 194 (12–16) (2005) 1527–1555.
[17] Z. Qiu, X. Wang, Parameter perturbation method for dynamic responses of structures with uncertain-but-bounded parameters based on interval analysis, *International Journal of Solids and Structures* 42 (18–19) (2005) 4958–4970.
[18] S. McWilliam, Anti-optimization of uncertain structures using interval analysis, *Computer & Structures* 79 (4) (2001) 421–430.
[19] I. Elishakoff, Three version of the finite element method based on concepts of either stochasticity, fuzziness, or anti-optimization, *(ASME) Applied Mechanical Review* 51 (3) (1998) 209–218.
[20] G. Manson, Calculating frequency response functions for uncertain systems using complex affine analysis, *Journal of Sound and Vibration* 288 (3) (2005) 487–521.
[21] C.Z. Qiu, X. Wang, Comparison of dynamic response of structures with uncertain-but-bounded parameters using non-probabilistic interval analysis method and probabilistic approach, *International Journal of Solids and Structures* 40 (20) (2003) 5423–5439.
[22] B.S.L.P. de Lima, N.F.F. Ebecken, A comparison of models for uncertainty analysis by the finite element method, *Finite Elements in Analysis and Design* 34 (2) (2000) 211–232.
[23] I. Elishakoff, M. Zingales, Contrasting probabilistic and anti-optimization approaches in an applied mechanics problem, *International Journal of Solids and Structures* 40 (16) (2003) 4281–4297.
[24] R.E. Moore, *Interval Analysis*, Prentice-Hall, Englewood Cliffs, NJ, 1966.
[25] E.R. Hansen, *Global Optimization Using Interval Analysis*, Marcel Dekker, New York, 1992.